Probing the intrinsic optical Bloch-mode emission from a 3D photonic crystal

You may also be interested in:

Experimental observation of anomalous thermal radiation from a three-dimensional metallic photonic crystal
Mei-Li Hsieh, Shawn-Yu Lin, James A Bur et al.

A wafer-scale backplane-assisted resonating nanoantenna array SERS device created by tunable thermal dewetting nanofabrication
Te-Wei Chang, Manas Ranjan Gartia, Sujin Seo et al.

Nanostructure arrays in free-space: optical properties and applications
Stéphane Collin

Compact antireflection structures for photonic crystals
Zhaofeng Li, Ekmel Ozbay, Haibo Chen et al.

Tailoring light–matter coupling in semiconductor and hybrid-plasmonic nanowires
Brian Piccione, Carlos O Aspetti, Chang-Hee Cho et al.

Roadmap on optical energy conversion
Svetlana V Boriskina, Martin A Green, Kylie Catchpole et al.

Probing the intrinsic optical Bloch-mode emission from a 3D photonic crystal

Mei-Li Hsieh[1,2]**, James A Bur**[2]**, Qingguo Du**[3]**, Sajeev John**[3] **and Shawn-Yu Lin**[2]

[1] Department of Photonics, National Chiao-Tung University, Hsinchu, Taiwan
[2] Department of Physics, Applied Physics and Astronomy, Rensselaer Polytechnic Institute, Troy, NY 12180, USA
[3] Department of Physics, University of Toronto, 60 St George Street, Toronto, Ontario, M5S 1A7, Canada

E-mail: sylin@rpi.edu

CrossMark

Abstract

We report experimental observation of intrinsic Bloch-mode emission from a 3D tungsten photonic crystal at low thermal excitation. After the successful removal of conventional metallic emission (normal emission), it is possible to make an accurate comparison of the Bloch-mode and the normal emission. For all biases, we found that the emission intensity of the Bloch-mode is higher than that of the normal emission. The Bloch-mode emission also exhibits a slower dependence on $(\hbar\omega/k_b T)$ than that of the normal emission. The observed higher emission intensity and a different T-dependence is attributed to Bloch-mode assisted emission where emitters have been located into a medium having local density of states different than the isotropic case. Furthermore, our finite-difference time-domain (FDTD) simulation shows the presence of localized spots at metal–air boundaries and corners, having intense electric field. The enhanced plasmonic field and local non-equilibrium could induce a strong thermally stimulated emission and may be the cause of our unusual observation.

(Some figures may appear in colour only in the online journal)

Recent advances in nanotechnology have made it possible to make complex nanostructures that are capable of altering the conventional thermal-radiation characteristics of a hot object [1, 2]. Conventional thermal radiation is broadband, non-coherent, obeys the T-dependence of Bose–Einstein distribution and is well described by Planck's blackbody radiation law [3, 4]. Two most well-known examples are blackbody radiation from the Sun and greybody radiation from a tungsten light bulb. Nano-engineering of a metallic object introduces optical resonances and feedback, producing significant modification of thermal radiative properties beyond Planck's law. For example, optical coherence and emission directionality has been observed in a heated 1D grating and 3D photonic crystal (PC) structures [5, 6]. Radiation linewidth narrowing and intensity enhancement have been predicted in a meta-material [7, 8]. In addition, modified thermal emission has been reported in the near and mid-infrared wavelength using 2D PC [9–11]. Furthermore, in a cavity/PC structure, it has been observed that thermal-radiation intensity can exceed the Planck's limit and its T-dependence deviates from Bose–Einstein distribution [12–14]. However, the sample's temperature in this study is determined from a reference blackbody-radiation spectrum, which may cause uncertainty in T-measurement.

In this paper, we show an alternative way to determine the temperature of a heated PC-filament at a given electrical bias. We further show that it is possible to obtain the intrinsic Bloch-mode emission reliably. From the determined emission intensity and sample-T, we show that T-dependence of the intrinsic Bloch-mode emission can deviate from Bose–Einstein distribution. Our FDTD simulation shows the presence of local hot spots at metal–air boundaries and corners, indicating that extreme field enhancement and exceptional electromagnetic local density of states (LDOS) may stimulate a stronger emission than that from a conventional blackbody object.
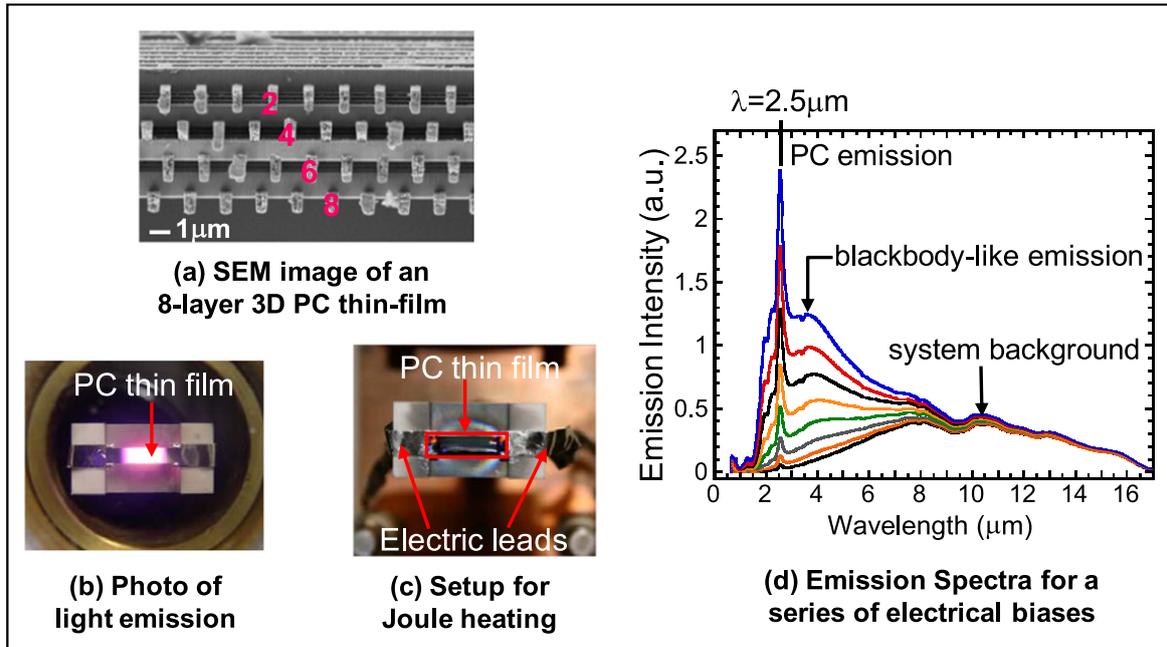
Figure 1. (**a**) A scanning-electron-micrograph image of our PC sample, which is a free-standing thin film ∼6 μm thick. (**b**) A photo of light emission from a PC sample. (**c**) A photo of the PC thin film, the ceramic mount and the electrical contact leads. (**d**) Emission spectra taken from a PC sample electrically biased at a series of current, $I = 0.325$–0.50 A with an 0.025 A increment.

The 3D PC sample that we used consists of eight layers of 1D tungsten rods with diamond lattice symmetry [15]. The 1D rod width, rod height and rod-to-rod spacing are w = 0.5 μm, h = 0.75 μm and a = 1.5 μm, respectively [12]. Figure 1(a) shows a scanning-electron-micrograph image of our PC sample, which is a free-standing thin film about 6 μm thick. To achieve thermal emission, the sample is heated electrically through Joule heating [2]. To minimize thermal conduction and convection, the sample is mounted on a ceramic mount and placed inside an optical dewar in vacuum. Figure 1(b) shows a photo of light emission from a PC sample. Figure 1(c) shows a photo of the PC thin film, the ceramic mount and the electrical contact leads.
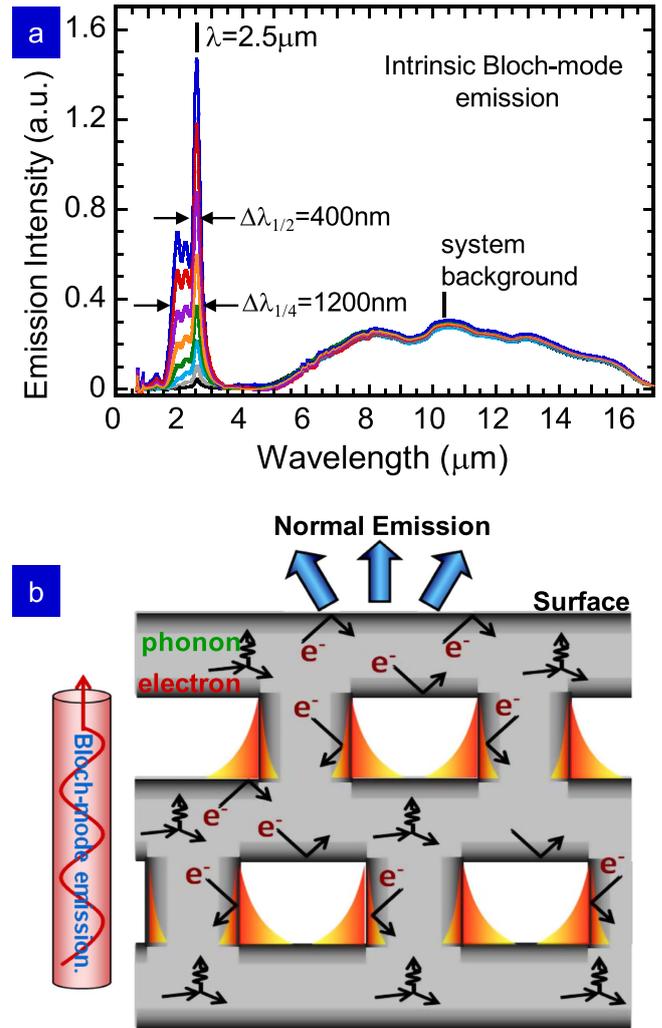
Figure 1(d) shows emission spectra taken from a PC sample electrically biased at a series of current, $I = 0.325$–0.50 A with an $\Delta I = 0.025$ A increment. The spectrum contains three peaks. The first is a sharp one at $\lambda = 2.5$ μm and is independent of bias-I. This is attributed to band-edge Bloch-mode emission. The second is a broader peak. As bias-I is increased, the peak position shifts to shorter wavelength from $\lambda \sim 4.5$ μm to $\lambda \sim 3.5$ μm and the peak intensity is also increased. This is attributed to the 'normal emission'. This portion of radiation originates from collisions of hot electrons with phonons at and near the external surface of a PC sample. Since it is coupled into free space, it has a conventional form of greybody radiation spectrum. The black dashed curve indicates a conventional thermal-radiation spectrum. The last one is also a broad peak. However, its peak position is fixed at $\lambda \sim 10$ μm and peak emission intensity is independent of bias-I. This signal is the system background from the Fourier transform infrared (FTIR) spectrometer.

Figure 2(a) shows results of the fitting analysis of a PC-emission spectrum biased at $I = 0.5$ A. The blue, black and red curves represent the total measured spectrum, the black-body curve and the PC spectrum, respectively. The optimized fitting is obtained by adjusting the blackbody curve (or emissivity of a greybody) such that it fits well to the total spectrum in the peak emission regime at $\lambda = 3$–5 μm (the yellow region). The fitting yields a deduced PC spectrum (the red curve), having a near-zero intensity at $\lambda = 3$–5 μm and is well separated from system background $\lambda \sim 10$ μm. By Wien's displacement law [16], the fitting also yields the sample's surface temperature of $T_{ss} = 900$ K. At $\lambda = 2.5$ μm, the ratio of Bloch-mode emission to normal emission is $I_{PC}/I_0 = 1.7 \pm 0.1$. So, the Bloch-mode emission is stronger than the normal emission at $T_{ss} = 900$ K. Given the satisfactory separation of the PC spectrum from the blackbody curve, we repeat the fitting study for all biases. Figure 2(b) shows emission spectrum taken at $I = 0.45$ A. Again, the deduced PC spectrum has a near-zero intensity at $\lambda = 3$–5 μm and is well separated from the background. At this bias, the blackbody curve yields a lower value of $T_{ss} = 800$ K. Meanwhile, the ratio of Bloch to normal emission at $\lambda = 2.5$ μm is increased to $I_{PC}/I_0 = 2.1 \pm 0.1$. So, Bloch-mode emission is even stronger than the normal emission at $T_{ss} = 800$ K. Figure 2(c) shows emission spectrum taken at $I = 0.40$ A. Correspondingly, the sample's surface T_{ss} is reduced to $T_{ss} = 700$ K. At this relatively lower bias, the intensity ratio is further increased to $I_{PC}/I_0 = 2.9 \pm 0.15$. This trend of increasing (I_{PC}/I_0) ratio for decreasing biases, or lower thermal excitation, continues. And, at the lowest bias of $I = 0.325$ A, we found an intensity ratio of $I_{PC}/I_0 = 5.0 \pm 0.2$.
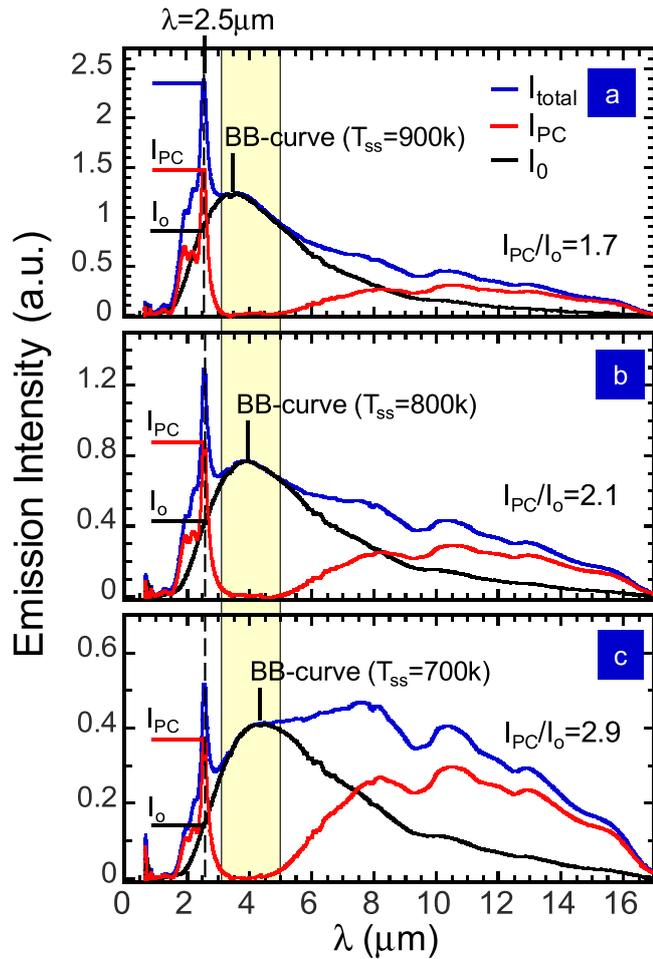
Figure 2. (a) The results of fitting analysis of a sample spectrum biased at $I = 0.5$ A. The blue, black and red curves represent the total measured spectrum, the blackbody spectral function at $T_{ss} = 900$ K and the PC spectrum, respectively. (**b**) and (**c**) Emission spectrum taken at $I = 0.45$ and 0.4 A, respectively. The corresponding sample temperatures are $T_{ss} = 800$ and 700 K, respectively.

Figure 3. (a) A summary of the PC spectrum for all biases. The FWHM of the PC emission is only $\Delta\lambda = 400$ nm. (**b**) A schematic drawing of different energy dissipation mechanisms that lead to heating of the PC sample as well as normal and Bloch-mode emission.

A summary of the successful fitting analysis and the resulting PC spectra are shown for all biases in figure 3(a). Note that the emission signal is near zero at $\lambda = 3$–5 μm for all biases (the yellow region shown in figure 2). Also, the system background remains the same for all biases, as expected. These two points indicate that our blackbody curve fitting/subtraction is successful in isolating the PC spectrum from the system background and also from the blackbody-like 'normal emission'. Therefore, the observed PC spectrum is a pure emission from the intrinsic Bloch-mode at the photonic band edge of $\lambda \sim 2.5$ μm. To the best of our knowledge, this is the first truly clean Bloch-mode thermal emission that has been observed. Note that the full width at half maximum (FWHM) of the intrinsic PC emission at $T_{ss} = 900$ K (inferred from normal emission) is only $\Delta\lambda = 400$ nm. This is to be compared to $\Delta\lambda \sim 4$ μm for a blackbody emission at $T_{ss} = 900$ K. In addition, the PC emission intensity (I_{PC}) at $\lambda = 2.5$ μm is stronger than that of the normal emission (I_0) for all biases.

The underlining physical process of the observed emission may be understood by considering electronic scattering in a metallic nanostructure. In our electrically biased metallic PC sample, energy from electrical current in the PC can be dissipated in at least three ways [17]. A schematic is shown in figure 3(b) to illustrate the different dissipation mechanisms. First, electronic scattering from phonons in the metal will contribute to the measured T of the sample. Second, electronic scattering from or near the surface of the sample contributes to conventional forms of radiation into the featureless electromagnetic vacuum of free space (the blue arrows). This accounts for the observed 'normal emission', which follows a blackbody-like spectrum. From the blackbody curve and Wien's displacement law, the sample's surface T_{ss} is determined. Essentially, this normal emission serves as an internal T-sensor and is a direct measure of the sample's temperature. Third, electronic collisions with the interior surfaces of the nano-structured filament may excite localized surface plasmon resonances that emit light into the engineered
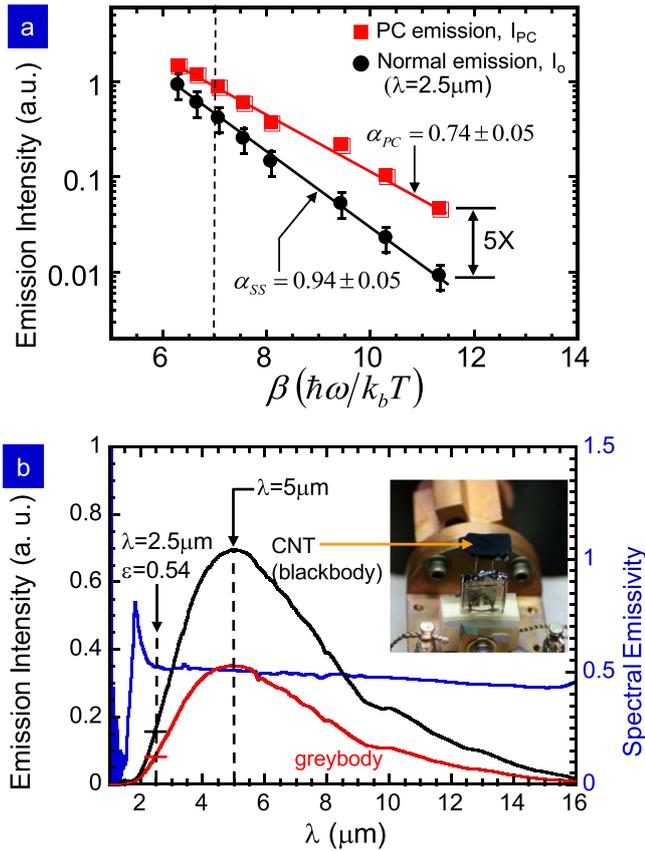
Figure 4. (a) A summary of emission intensity at $\lambda = 2.5\,\mu$m as a function of $\beta = (\hbar\omega/k_B T_{ss})$ in a semi-logarithmic plot. For all biases, Bloch-mode emission is stronger than the normal emission. Also, both the Bloch-mode and normal emission follow a straight line, indicating an exponential dependence, i.e. $e^{-\alpha(\hbar\omega/k_B T_{ss})}$. (**b**). Tungsten's normal emission (red curve), a blackbody mission (black curve) and tungsten's directional spectral emissivity (blue curve) taken at $T_{ss} = 600$ K.

electromagnetic vacuum. This is particularly pronounced in the presence of optical pass bands within a photonic band gap (PBG) [17]. Even in the absence of a complete 3D PBG, metallic edges and corners can provide hot spots for light emission into slow-light modes of the PC. This is the physical origin of the 'Bloch-mode emission' we observe.

To gain further insight into the nature of emission from PC, we examine its *T*-dependence. Figure 4(a) summarizes the emission intensity at $\lambda = 2.5\,\mu$m as a function of $\beta = (\hbar\omega/k_B T_{ss})$ in a semi-logarithmic plot. For all biases, Bloch-mode emission is stronger than the normal emission. Because normal emission is only a greybody emission with a finite emissivity, this comparison does not necessarily suggest that Bloch-mode emission exceeds the Blackbody limit. The data also show that both the Bloch and normal-emission data follow straight lines, indicating an exponential dependence, i.e. $e^{-\alpha(\hbar\omega/k_B T_{ss})}$. For the normal emission, $\alpha = 0.94 \pm 0.05$ and is close to unity. So, the normal emission is a blackbody-like emission that follows Boltzmann–Einstein distribution. For the Bloch-mode emission, we find $\alpha = 0.74 \pm 0.05$, which is much less than one. The reason for the different emission behavior may be due to non-equilibrium effects or some novel quasi-equilibrium between the tungsten

oscillators and the radiated energy. A more detailed explanation will be discussed later.

To determine tungsten's surface emissivity, we measure a tungsten normal emission and a reference blackbody emission at the same temperature. Figure 4(b) shows tungsten's normal emission (red curve), a blackbody emission (black curve) and tungsten's directional spectral emissivity (blue curve) at $T_{ss} = 600$ K. The blackbody emission is taken from a super-dark carbon nanotube array, having an emissivity of $\varepsilon = 0.9997$ [18]. A photo of the super-dark material is shown in the inset of figure 4(b). Tungsten's high-*T* emissivity is determined to be $\varepsilon = 0.45$–0.55 for $\lambda = 2$–$16\,\mu$m. This emissivity value is within the range reported elsewhere [19–22]. The data for $\lambda < 2\,\mu$m is noisy due to a weak signal. Taking into account an emissivity of $\varepsilon = 0.5 \pm 0.05$, the Bloch-mode emission still exceeds the blackbody limit at the low-*T* regime i.e. $(\hbar\omega/k_B T_{ss}) \geqslant 6.5$. However, this statement is precise only when there is a well-defined equilibrium *T*. We first note that there is just a single temperature, T_{ss}, in our sample system. And, the Bloch-emission peak at $\lambda = 2.5\,\mu$m is like a non-equilibrium laser-like emission that cannot be described by a temperature [14, 17]. Therefore, we may only conclude that, under the same heating condition (not the same *T*), Bloch emission is stronger than blackbody emission at low thermal excitation limit. Nonetheless, the mechanism that drives Bloch emission is unique, i.e. excitation by localized surface Plasmon into an engineered slow-light mode of a PC. The consequence is a stronger and narrower Bloch-emission peak at $\lambda = 2.5\,\mu$m.

There are at least two contributing factors to the observed enhancement of radiation. One is the strong plasmonic field at the air–metal interfaces and the other localized hot spots inside the sample structure. To examine electromagnetic (EM) field distribution inside the interior surface of our sample, we perform FDTD calculation at resonant-λs. Plane waves were incident from the top and coupled into the sample.

Figure 5(a) shows computed reflection spectra for the PC sample for TE (blue curve) and TM (red curve) polarization, respectively. The inset shows computed (solid line) and measured (dashed line) reflectance spectra for $\lambda = 1.5$–$3.5\,\mu$m. At $\lambda \approx 1.8\,\mu$m and $\lambda \approx 2.4\,\mu$m, reflection minimum occurs indicating strong coupling of light to the sample at these λs. Figure 5(b) shows the results of the computed field distribution at $\lambda = 1.8, 1.9, 2.4$ and $2.5\,\mu$m. Electric field (E-field) strength is color coded in a linear scale. For $\lambda = 1.8\,\mu$m, E-fields are strongly concentrated at the corners of air–metal boundaries (indicated by red circles). Similarly, for $\lambda = 2.4\,\mu$m, the E-fields are strongly enhanced at the air–metal interfaces (indicated by red ovals) and also inside the interior of the PC sample. To further quantify the field enhancement, figures 5(c) and (d) show the E-field as a function of distance along the dashed lines for $\lambda = 1.8$ and $2.4\,\mu$m, respectively. At $\lambda = 1.8\,\mu$m, the E-field is enhanced by as much as 100 times, or its intensity is enhanced by 10 000 times. At $\lambda = 2.4\,\mu$m, the E-field is enhanced by 5–6 times, or its intensity is enhanced by 25–36 times. These results indicate the presence of localized regions where the E-field is the strongest and surface plasmon resonances can be
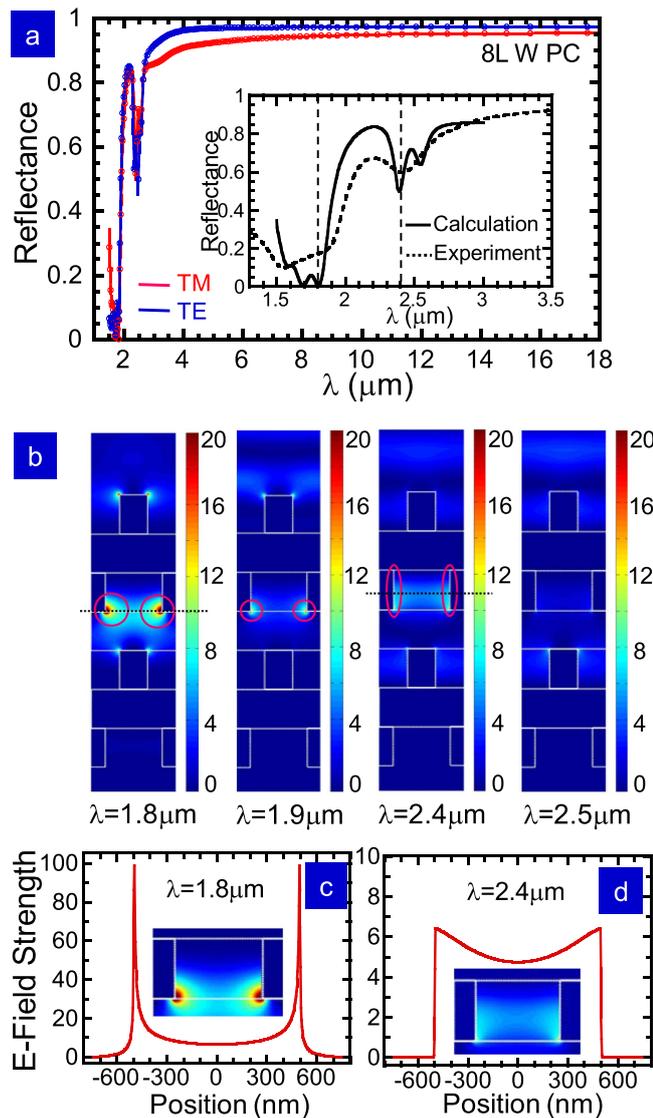
Figure 5. (a) Computed reflection spectra for the PC sample for TE (blue curve) and TM (red curve) polarization, respectively. The inset shows computed (solid line) and measured (dashed line) reflectance spectra for $\lambda = 1.5$–$3.5 \ \mu$m. At $\lambda \approx 1.8 \ \mu$m and $\lambda \approx 2.4 \ \mu$m, reflection minimum occurs indicating strong coupling of light to the PC sample. (**b**) Results of the computed field distribution at $\lambda = 1.8$, 1.9, 2.4 and 2.5 μm. Plane waves were incident from the top and coupled into the sample. E-field strength is color coded in a linear scale. (**c**), (**d**) E-field as a function of distance along the dashed lines for $\lambda = 1.8$ and 2.4 μm, respectively.

excited to emit light. A preliminary estimation, based on the strength of field-concentration, indicates that it is possible to induce a significant thermally stimulated radiation in our PC sample [23][4].

---

[4] Let us compare the spontaneous emission A_{21} and thermally stimulated emission $B_{21}\overline{W}(\omega)$ rate, where $A_{21}/B_{21}\overline{W}(\omega) = 1/\overline{n} = \exp{(\hbar\omega/k_B T)} - 1$ in equilibrium [19]. Here, A_{21}, B_{21} and $\overline{W}(\omega)$ are Einstein's A, B coefficients and the mean radiative energy density by Planck's law. For $\hbar\omega/k_B T = 7$, $A_{21}/B_{21}\overline{W}(\omega) = \exp{(7)} - 1 = 1095$. So, thermally stimulated emission is weaker than spontaneous emission rate. However, in the presence of strong field concentration of 50–100 times at air-metal interface, the local energy density at resonant-ω is enhanced by 2500–10 000 times. Therefore, thermally stimulated emission is enhanced by 2500–10 000 and exceeds spontaneous emission rate.

While the field-concentration argument explains the observed emission enhancement, it does not predict its dependence on $(\hbar\omega/k_B T_{ss})$ as shown in figure 4(a). The existence of local hot spots in our sample and a resulting hotter radiation temperature for Bloch-mode emission offers one possible explanation and may be understood as follows. Local hot spots may exist in the interior air–metal boundary regions for two reasons. First, it can occur when the radiation rate is enhanced such that the radiative lifetime becomes comparable to the time scale of electron–phonon coupling of a few psec [24, 25] or phonon transport time of ∼50–100 psec in our 1D tungsten rods[5] [26–28]. Second, it can occur when there is strong recycling and feedback of energy from the open, interior space of the structure to the air–metal boundary from slow-light modes of the PC. Last, it is also noted that isotropy is broken by the presence of localized LDOS in our PC structure. The combination of strongly enhanced EM fields and hotter regions at the interior air–metal interfaces and corners may be responsible for the strongly enhanced Bloch-mode emission.

In summary, we studied intrinsic Bloch-mode and normal emission from a heated 3D tungsten PC sample as a function of electric bias and temperatures. We found that Bloch-mode emission is stronger than normal emission for all biases and, especially at low temperatures, $T_{ss} < 800$ K. From a T-dependence study, we also found that Bloch-mode thermal emission follows a different exponent than the normal-emission case. Our FDTD simulation shows the presence of local high-field regions at metal–air boundaries and corners, indicating that strong plasmonic field and local non-equilibrium may stimulate a stronger emission than that from a conventional blackbody object.

Acknowledgments

References

[1] Fleming J G *et al* 2002 *Nature* **417** 52–5
[2] Lin S Y *et al* 2003 *Appl. Phys. Lett.* **83** 593–5
[3] Kirchhoff G 1860 *Philosophical Magazine Series* 4 **20** 1–21
[4] Planck M 1912 *The Theory of Heat Radiation* (New York: Dover)
[5] Greffet J J *et al* 2002 *Nature* **416** 61–4
[6] Hsieh M L *et al* 2013 *Opt. Lett.* **38** 911–3

---

[5] Speed of sound in bulk tungsten material is 3–5 nm/psec at room temperature [26]. Although there is no direct measurement of acoustic phonon speed in tungsten, acoustic photon speed in other solids, such as aluminum and silica, has been found to be 5–7 nm/psec [27, 28]. Given the acoustic phonon speed, the excited phonons would take ∼100 psec to move across a 1D tungsten rod of 500–700 nm size in our sample.

[7] Nefedov I S and Melnikov L A 2014 *Appl. Phys. Lett.* **105** 161902

[8] Liu X *et al* 2011 *Phys. Rev. Lett.* **107** 045901

[9] Chan D L C *et al* 2006 *Opt. Exp.* **14** 8785–96

[10] Maruyama S *et al* 2001 *Appl. Phys. Lett.* **79** 1393–5

[11] Inoue T *et al* 2013 *Appl. Phys. Lett.* **102** 191110

[12] Hsieh M L *et al* 2015 *Nanotechnology* **26** 234002

[13] Chow W W 2006 *Phys. Rev.* A **73** 013821

[14] Kaso A and John S 2007 *Phys. Rev.* A **76** 53838

[15] Lin S Y *et al* 1998 *Nature* **394** 251

[16] Dereniak E L and Boreman G D 1996 *Infrared Detectors and Systems* (New York: Wiley) ch 2

[17] John S and Wang R 2008 *Phys. Rev.* A **78** 043809

[18] Yang Z P *et al* 2008 *Nano Lett.* **8** 446–51

[19] Thomas L K 1968 *J. App. Phys.* **39** 4681

[20] Matsumoto T *et al* 1999 *Int. J. Thermophysics* **20** 943

[21] Cagran C *et al* 2005 *Int. J. Thermophysics* **26** 1001

[22] Brodu E *et al* 2015 *Acta Mater.* **84** 305

[23] Loudon R 1983 *The Quantum Theory of Light* 2nd edn (New York: Oxford University Press) ch 1, p 17

[24] Brorson S D *et al* 1990 *Phys. Rev. Lett.* **18** 2172

[25] Shen A *et al* 2015 *Phys. Rev.* B **91** 045129

[26] Lide R D (ed) 2013 *CRC Handbook of Chemistry and Physics* 84th edn (Boca Raton, FL: CRC)

[27] Klieber C *et al* 2011 *Appl. Phys. Lett.* **98** 211908

[28] Tas G and Moris H 1994 *J Phys. Rev.* B **49** 15046